Attributed Scattering Centers for SAR ATR

Lee C. Potter, *Member, IEEE,* and Randolph L. Moses, *Senior Member, IEEE*

***Abstract*— High-frequency radar measurements of man-made targets are dominated by returns from isolated scattering centers, such as corners and flat plates. Characterizing the features of these scattering centers provides a parsimonious, physically relevant signal representation for use in automatic target recognition (ATR). In this paper, we present a framework for feature extraction predicated on parametric models for the radar returns. The models are motivated by the scattering behavior predicted by the geometrical theory of diffraction. For each scattering center, statistically robust estimation of model parameters provides high-resolution attributes including location, geometry, and polarization response. We present statistical analysis of the scattering model to describe feature uncertainty, and we provide a least-squares algorithm for feature estimation. We survey existing algorithms for simplified models, and derive bounds for the error incurred in adopting the simplified models. A model order selection algorithm is given, and an M-ary generalized likelihood ratio test is given for classifying polarimetric responses in spherically invariant random clutter.**

I. Introduction

THE high-frequency scattering response of a distributed object is well approximated as a sum of responses from individual scatterers, or scattering centers [1]. These scatterers provide a physically relevant, yet concise, description of the object and are thus good candidates for use in automatic target recognition (ATR) [2]–[7]. Beyond ATR applications, attributed scattering centers provide high-resolution analysis of scattering for data compression [8], for radar cross section reduction in stealth design, and for elimination of spurious scattering in compact ranges [9]. In this paper, we present scattering models and statistical estimation techniques to extract attributed scattering centers for use as discriminants in ATR. Attributes for each scattering center include high-resolution downrange and crossrange locations, amplitude, frequency dependence (partially characterizing scattering center geometry), and polarimetric properties.

Scattering center attributes are estimated as parameters in a model of radar scattering. The use of scattering models in conjunction with statistical estimation permits us to quantify uncertainty, which is needed for Bayesian evidence accrual in target discrimination and identification. Attribute uncertainty is described as a function of radar system characteristics such as bandwidth and target-to-clutter ratio. Furthermore, statistical analysis of attribute uncertainty provides bounds on achievable performance; these bounds are independent of estimation algorithm.

Fig. 1 illustrates the use of attributed scattering centers for radar signature analysis. The figure shows an inverse synthetic aperture radar (ISAR) image of a pickup truck computed from stepped frequency measurements (specifically, the GTRI K-band ISAR, 1 ft $\times$ 1 ft resolution, 5.5° depression, 119.2° azimuth). Radar illumination is from the top of the image. The traditional ISAR image is shown in pseudo-color; the superimposed icons show the dominant scattering centers extracted from the radar phase history using a model-based estimator. Each scattering center has an associated subpixel location, amplitude, phase, frequency dependence, and polarimetric signature. Ground truth is unavailable for the target; however, 70.1% of the entire image energy is modeled by the six estimated scattering centers. This introductory example is given as a notional illustration of a scattering center description. Descriptions of the scattering attributes and examples computed from measurements of known objects are given in subsequent sections.

The use of simplified scattering center models is well established for high-resolution radar imaging [10]–[14] and for estimation of location and amplitude of dominant scattering mechanisms [3], [15]–[17]. Our proposed set of attributes expands the target description to more fully exploit phenomenology observable as a function of frequency, aspect, and polarization. Significantly, diverse scattering behavior across wavelength and polarization has become accessible with the emergence of both ultrawideband (UWB) and fully polarimetric sensors. We adopt a statistical estimation framework that provides estimates of feature uncertainty. Used in conjunction with other features, such as shadows, context, and image texture, attributed scattering center features hold promise for both feature-based [18] and model-based [19] ATR systems.

The remainder of the paper is organized as follows. In Section II we present a parametric scattering model based on the geometric theory of diffraction (GTD) and describe a maximum likelihood (ML) estimation algorithm. We characterize feature uncertainty with statistical analysis of parameter variance as a function of system parameters. In Section III, we survey simplified models for radar scattering. For both the damped and undamped exponential signal models we relate the model parameters to the scattering center attributes parameterized by GTD-based model. We bound the approximation error, review algorithms for estimating the model parameters, and highlight parameter estimation issues arising from use of the simplified models. Additionally, we present an order-selecting maximum likelihood estimation algorithm addressing the critical issue of model order for target classification. In Section IV we discuss polarization attributes of scattering centers and

Manuscript received November 1, 1995; revised July 30, 1996. This research was supported in part by the Advanced Research Project Agency under Contract MDA972-93-1-0015 managed through Wright Laboratories, and by the Army Research Laboratory under Contract DAAL01-93-0095.

The authors are with the Department of Electrical Engineering, The Ohio State University, Columbus, OH 43210 USA (e-mail: potter@ee.eng.ohio-state.edu).

Publisher Item Identifier S 1057-7149(97)00462-4.

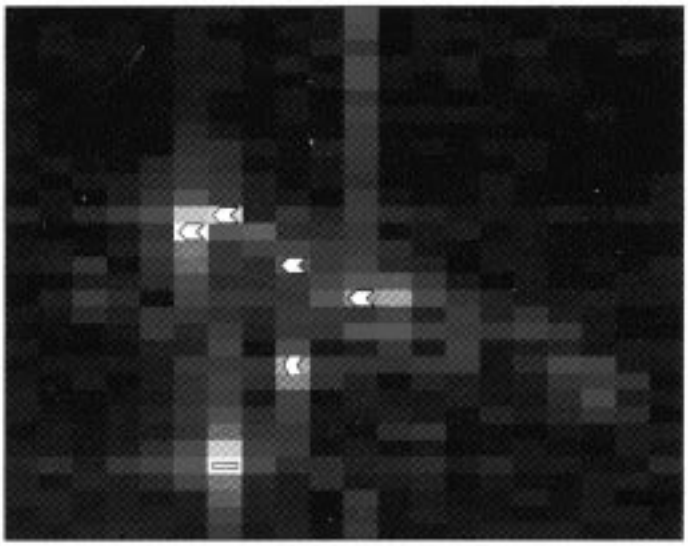

Scattering center attributes
Position = (3.19 m, 3.25 m)
Amplitude = $148\angle -14^{\circ}$
$\alpha = 1$ (see Table 1)
Dihedral; tilt = -37°

Fig. 1. Scattering center description of a SAR image represents the target as a collection of estimated scattering centers. The table shows attributes for the right-most scattering center.

present an M-ary hypothesis test for classifying polarimetric responses measured in spherically invariant random clutter. Concluding remarks are presented in Section V.

II. Physics-Based Scattering Center Model

The synthetic aperture radar (SAR) sensor gives access to information about a target and pose through the phase history, which is a complex-valued function of frequency, aspect angle, and polarization. For analysis of the received signal, we adopt a parametric scattering model based on the geometrical theory of diffraction.

A. Scattering Model

Let the incident field be a plane wave propagating in the $+\hat{z}$ direction as shown in Fig. 2. From the geometrical theory of diffraction (GTD) [1] and its uniform version [20], if the wavelength of the incident excitation is small relative to the target extent, then the backscattered field appears to originate from a set of discrete scattering centers. The backscatter can be accurately approximated [21] by

$$\vec{E}^s(f,\theta,t) \approx \frac{\vec{E}_0}{ct} e^{j2\pi ft} \sum_{m=1}^{M} S_m(f,\theta) \exp\{-j2\pi f t_m\} \quad (1)$$

where f is frequency in Hertz, c is the propagation velocity, θ is the target aspect angle, and $t_m = \frac{2}{c}\vec{r}_m \cdot \hat{z} = \frac{2}{c}(x_m \cos\theta + y_m \sin\theta)$ is the round-trip propagation delay of the mth scattering center. The amplitude $S_m(f,\theta)$ is a frequency

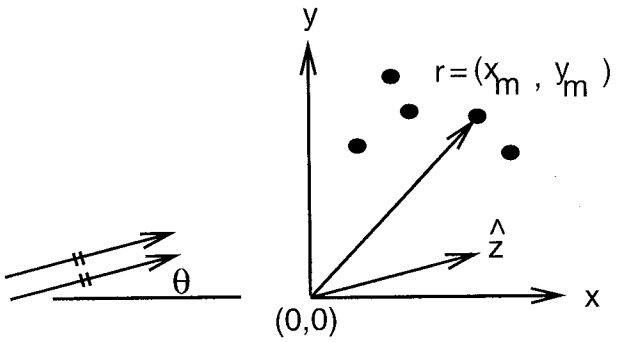

Fig. 2. Sensor and target geometry.

and angle dependent coefficient determined by geometry, composition, and orientation of the scattering mechanism. Here the approximation $|ct - \hat{z} \cdot \vec{r}_m| \approx |ct|$ is invoked by assuming both far-field backscatter and scattering centers close to the origin. The corresponding normalized field for a given polarization (suppressing the $e^{j2\pi ft}$ time convention)

$$E(f,\theta) = \sum_{m=1}^{M} S_m(f,\theta) \exp\left\{\frac{-j4\pi f}{c}(x_m \cos\theta + y_m \sin\theta)\right\} \quad (2)$$

where x_m and y_m are the slant-plane downrange and cross-range locations of the mth scattering center.

For frequency dependence, the GTD predicts that scattering amplitude is of the form $(jf)^{\alpha_m}$ where α_m is an integer multiple of $\frac{1}{2}$. Table I summarizes the α parameters, and hence frequency dependencies, of five example scattering mechanisms; for multiple-bounce scattering, the frequency dependencies are multiplicative.

For many man-made scatterers, the dependence of $S_m(f,\theta)$ on angle is well approximated as a combination of sinclike terms. For example, the angle dependence of the GTD scattering amplitude for a strip of length d is given [1] by

$$\cos\left(d\frac{2\pi f}{c}\cos\theta\right) \pm jd\frac{2\pi f}{c}\mathrm{sinc}\left(d\frac{2\pi f}{c}\cos\theta\right). \quad (3)$$

However, no simple but widely applicable model similar to (3) is presently available; different forms of the angle dependence appear for different canonical scattering geometries. This difficulty motivates the use of a simpler but more universal model for angle dependence over small angle intervals. For narrow angles encountered in SAR imaging (e.g., 3° for 1-ft crossrange resolution at X-band), we choose to model the amplitude dependence as an exponential, $e^{\beta_m\theta}$. Thus, we adopt the following model for the backscattered electric field

$$E(f,\theta) = \sum_{m=1}^{M} A_m \left(\frac{jf}{f_c}\right)^{\alpha_m} e^{\beta_m\theta} \cdot \exp\left\{\frac{-j4\pi f}{c}(x_m \cos\theta + y_m \sin\theta)\right\} \quad (4)$$

where f_c is the center frequency. The model parameters $\{A_m, x_m, y_m, \alpha_m, \beta_m\}_{m=1}^{M}$ characterize the M individual scattering centers. For the mth scattering center, (x_m, y_m) gives the slant plane location with respect to a zero-phase reference, α_m characterizes the geometry, and hence frequency dependence, β_m characterizes the angular dependence of

TABLE I
TYPE PARAMETERS FOR CANONICAL SCATTERING MECHANISMS

Value of α	Example scattering geometries
1	flat plate at broadside; dihedral
$\frac{1}{2}$	singly curved surface reflection
0	point scatterer; doubly curved surface reflection; straight edge specular
$-\frac{1}{2}$	curved edge diffraction
-1	corner diffraction

scattering, and A_m is a complex scalar charactering the magnitude and phase.

If multiple transmit and receive polarization pairs are available, the GTD predicts the same angle and frequency dependence across polarizations but with a different amplitude [3], [15], [22]. Accordingly, the scattering measurement and amplitude coefficients are written as complex-valued vectors. For example, for a fully polarimetric radar using a horizontal and vertical polarization basis, the amplitude A_m is the complex-valued triple and the polarimetric measurements are modeled by

$$\begin{bmatrix} E_{HH}(f,\theta) \\ E_{HV}(f,\theta) \\ E_{VV}(f,\theta) \end{bmatrix} = \sum_{m=1}^{M} \begin{bmatrix} A_{HH,m} \\ A_{HV,m} \\ A_{VV,m} \end{bmatrix} \left(\frac{jf}{f_c}\right)^{\alpha_m} e^{\beta_m \theta} \cdot \exp\left\{\frac{-j4\pi f}{c}(x_m \cos\theta + y_m \sin\theta)\right\}. \tag{5}$$

The frequency-dependent behaviors in Table I can be inferred from single polarization data, with an uncertainty as discussed in Section II-B below. Multipolarization data provides further characterization of scattering mechanisms and can provide discrimination among mechanisms, as presented in Section IV.

The GTD is a high-frequency model, but remains highly accurate for objects of remarkably small electrical size, L/λ, where L is the object length and λ is the wavelength. Moreover, modeling accuracy degrades gracefully as L/λ decreases. For illustration, we compare the GTD prediction of frequency dependence in (4) to the analytically derived solution of scattering from an $L = 0.5$ m diameter perfectly conducting disk oriented 15° from normal to the radar line of sight. Stepped frequency samples are computed from 1 to 3 GHz with 10 MHz sample spacing. The disk and largest wavelength λ_0 are depicted in Fig. 3(a). The frequency range corresponds to disk electrical sizes from 5 wavelengths to only 1.67 wavelengths. Nonetheless, the GTD model differs from the exact analytical scattering solution by only 1.4% in root mean-square (RMS) error summed over the 201 frequency samples. The exact and modeled scattering are shown in Fig. 3(b); the small discrepancy is discernible near 0.5 m. At higher frequencies, the GTD model is even more accurate. Computation of a least-squares fit of the model in (4) correctly identifies the α values of the two edge diffractions ($\alpha = -0.5$ for Q_1 and Q_2) and two second-order diffraction mechanisms ($\alpha = -1$ for Q_1Q_2 and Q_3Q_4). The estimated locations and α values are depicted by the vertical bars in Fig. 3(b). The Q_1Q_2 and Q_3Q_4 mechanisms are separated by only 0.0008 Fourier

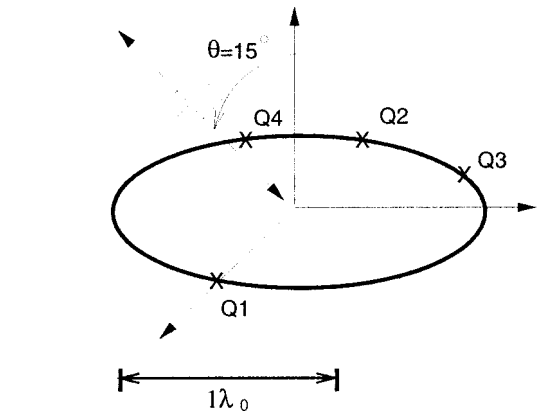

(a)

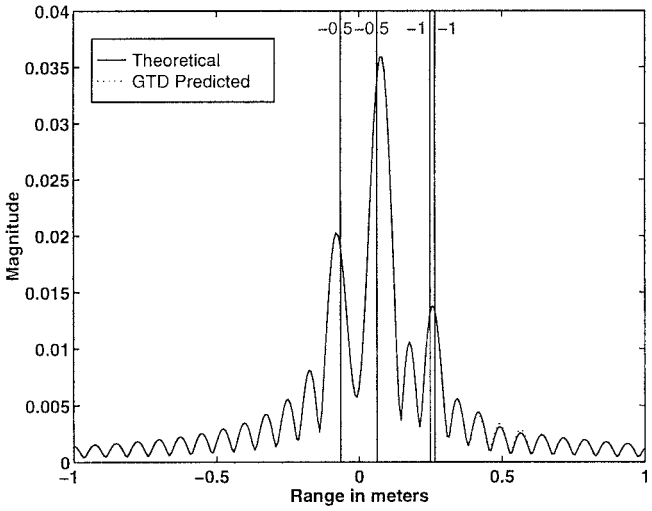

(b)

Fig. 3. GTD model accurately predicts frequency dependence.

bin in range and, hence, not resolvable by Fourier analysis, as seen in the figure. (One Fourier resolution bin$= \frac{c}{2\Delta f(2K)}$, which is 0.075 m for this example.) However, the two are resolved by the model-based analysis. The four scattering locations are estimated using the GTD-based model with an average range error of 0.065 Fourier bin.

Equation (4) represents a general scattering model, and forms the basis of all parametric scattering models we consider. In many applications, the radar measurements are sampled on a polar grid [23]

$$\begin{aligned} f_k &= f_c + k\,\Delta f, & k &= -K, \ldots, K \\ \theta_l &= \theta_0 + l\,\Delta\theta, & l &= -L, \ldots, L. \end{aligned} \tag{6}$$

It is desirable in many cases to consider scattered field measurements sampled on a rectilinear grid. The primary reason is that the phase term in (4) or (5) is nonlinear on a polar grid, but becomes linear on a rectilinear grid. Many estimation algorithms exploit linear phase for computational speed. If the total angular deviation $L\,\Delta\theta$ is small (so $\sin(L\,\Delta\theta) \approx L\,\Delta\theta$) and if the measurement frequency range is narrowband (so $K\,\Delta f \ll f_c$), then the polar grid is approximately equal to a rectilinear grid with spatial frequency axes f_x and f_y aligned

to the range and crossrange directions

$$\begin{aligned} f_{x,k} &\approx f_c + k\,\Delta f, & k &= -K,\ldots,K \\ f_{y,l} &\approx f_c \Delta\theta l, & l &= -L,\ldots,L. \end{aligned} \tag{7}$$

The resulting linear phase scattering model is given by

$$E(k,l) = \sum_{m=1}^{M} \tilde{A}_m \left(1 + \frac{\Delta f}{f_c} k\right)^{\alpha_m} e^{\beta_m \Delta\theta l} \cdot \exp\left\{\frac{-j4\pi f_c}{c}\left(\frac{\Delta f}{f_c} k x_m + \Delta\theta\, l y_m\right)\right\} \tag{8}$$

where $\tilde{A}_m = A_m j^{\alpha_m} e^{\beta_m \theta_0} e^{-j4\pi f_c/c}$. When the small angle or small fractional bandwidth assumptions do not hold, the phase terms must be resampled to lie on a rectilinear grid using, e.g., methods described in [24] and [25]. The amplitude terms $(f/f_c)^{\alpha_m}$ and $e^{\beta_m \theta}$ in (4) vary much more slowly than the phase term in (4) as functions of f and θ, and therefore the amplitude terms need not be resampled. The result is again a model with frequency and angle dependence as in (8) and linear phase increments.

B. Maximum Likelihood Estimation and Cramér–Rao Bound

Given the physically based scattering model in (8), the attributed scattering center analysis task is to determine the model parameters $\{A_m, x_m, y_m, \alpha_m, \beta_m\}_{m=1}^{M}$ from noisy samples of $E(f,\theta)$. A least-squares estimator for the model parameters entails a nonlinear, nonconvex minimization over a mixture of continuous and discrete variables. We have developed an algorithm for computing least-squares estimates of the scattering center attributes parameterized in (8). For additive white Gaussian noise, this estimator is a maximum likelihood estimator, and the estimates asymptotically achieve the Cramér–Rao (CR) bound. A detailed description of the algorithm and its application to scattering center estimation is presented in [28], and the corresponding parameter CR bounds are derived. Here, we summarize the important conclusions of [28].

The algorithm is an iterative descent procedure. Any local descent procedure relies on good initialization; bounds on initialization error using a fast eigendecomposition are provided in Theorem 1 below. Additionally, the combinatorially expensive search over 5^M possible sets of α parameters is avoided by using a continuous reparameterization [27] of the discrete α parameters, then mapping the continuous estimates into discrete values.

The statistical properties of the algorithm can be analyzed by considering the CR bound. The CR bound of the parametric model in (4) is derived in [28] and provides a lower bound on the variance of model parameters estimated in the presence of additive white Gaussian noise. The bound is valid, within modeling assumptions, for parameter variance using any unbiased estimation algorithm. We find that estimation algorithms achieve the CR bound for moderate signal strengths; hence, the bounds provide analytical predictions of uncertainty in estimation attributes [28].

From the analysis presented in [28], we distill four lessons that characterize the effect of system parameters on attribute uncertainty. The derivation parallels [29], [30], and the conclusions are similar to those drawn from statistical analysis of simplified scattering models [29]–[31]. In particular, we consider resolvability of scattering centers, uncertainty due to neighboring scattering centers, the effect of frequency sample spacing, Δf, and the role of fractional bandwidth in reliably estimating α.

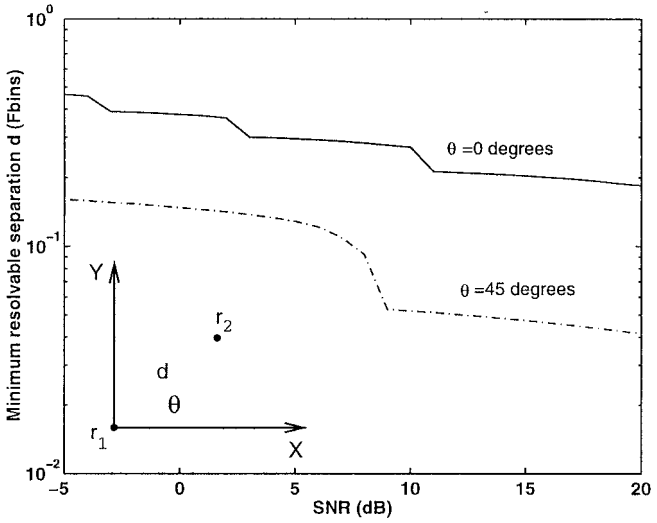

Fig. 4. Best- and worst-case resolution of two scattering centers using GTD-based ML algorithm.

First, we address resolution. A location estimate $r_m = (x_m, y_m)$ is asymptotically Gaussian with a 2×2 covariance bound Σ; Σ is determined from the CR bound for the continuous model parameters assuming known, discrete α_i parameters. Let σ_{90} define an ellipse

$$\left\{s : (r-s)^H \Sigma^{-1} (r-s) \le \sigma_{90}\right\}$$

containing 90% of estimates of scattering center location r_m. We define two scattering centers to be resolvable if their location variances are such that these 90% ellipses have no intersection. The resolution as a function of signal-to-noise ratio (SNR) is shown in Fig. 4. Since estimation uncertainty is affected by the orientation of the line segment between the two scattering centers with respect to the ellipse axes, we plot curves for the best and worst case orientations. We find that scattering centers 10 dB above the clutter background are resolvable to 0.27 Fourier bin (i.e., $0.27\frac{c}{2\Delta f(2K)}$). The geometry type, α, does not significantly affect the uncertainty of location estimates of equal energy scattering centers.

Second, while neighboring scattering centers affect parameter estimates, for separations exceeding two Fourier bins, two scattering centers may be considered isolated.

Third, for fixed fractional bandwidth, variance in both location and type estimates decreases linearly when sample spacing is reduced while retaining constant bandwidth.

Fourth, for isolated scattering centers and a fixed SNR, the sensor fractional bandwidth determines the reliability of α estimates. In general, reliable inference of geometric type from the frequency dependence of scattering increases with SNR or fractional bandwidth. We predict the reliability of the discrete α estimates by treating the α parameter as continuous, deriving

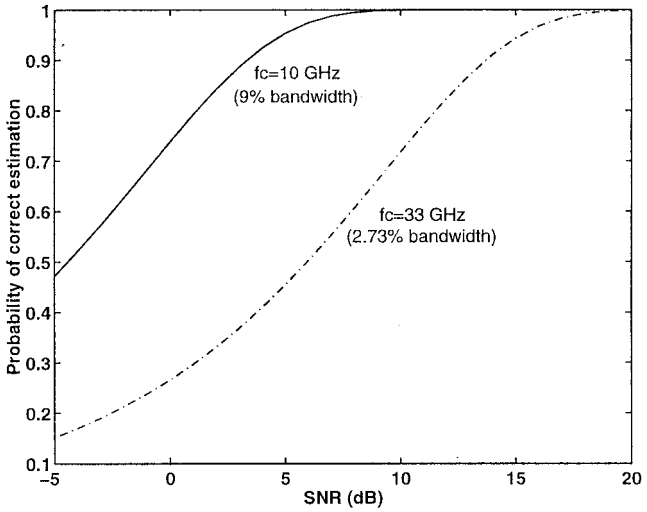

Fig. 5. Probability of correct type estimation using GTD-based ML algorithm for a radar with 1-ft. range resolution.

the Fisher information matrix (FIM) for the model parameters (including the α parameters), invoking the asymptotic normality of estimates, and using the inverse of the FIM to estimate the variance for the α parameter estimates; probabilities for the discrete types are then obtained by integrating the normal distributions. (Such predictions are within 3% of detection rates computed for simulated noisy scattering data [28].) The curves in Fig. 5 show the probability of correct α versus SNR for two fractional bandwidths. The lower curve is for 1-ft resolution at 33 GHz center frequency, while the upper curve is for 1-ft resolution at 10 GHz center frequency (2.73% and 9% fractional bandwidths, respectively). For example, from the figure we observe that for an isolated scattering center 6 dB above the background clutter, α estimation at 10 GHz cannot exceed 97.5% reliability, while accuracy for 33 GHz is limited to 50.2%.

III. Reduced Complexity Models

The algorithm in the previous section provides ML estimates of parameters directly from the GTD-based model in (8). The statistical accuracy of the estimated scattering attributes achieves the CR bound; however, the algorithm is computationally intensive, as it involves an iterative descent procedure. This motivates development of computationally less demanding algorithms that retain good statistical properties.

Computational efficiency can be gained by simultaneously considering reduced complexity models and corresponding reduced complexity estimation algorithms. One need not employ reduced complexity models, but instead can consider computationally simpler methods to estimate the parameters in (8). Such algorithms have been proposed in [32]–[36]. However, for many radar system operating specifications, the bias incurred by using a model simpler than (8) is small compared to the parameter variances. Thus, the benefit sought in adopting a reduced complexity model is availability of computationally efficient yet statistically accurate parameter estimation algorithms.

We thus consider approximations to (8) for reduced computational complexity. In particular, we consider both damped and undamped exponential signal models, which have been used extensively for radar signal analysis [11], [24], [2], [3], [37], [22], [17]. For each of these reduced complexity models, we present the parametric form, relate the parameters to the scattering center attributes parameterized by GTD-based model in (8), bound the approximation error, review algorithms for estimating the model parameters, and highlight parameter estimation issues arising from use of the surrogate models.

A. Damped Exponential Model

1) Scattering Model: First, we consider a sum of damped exponentials as a surrogate for the GTD-based scattering model. Let $E(k,l)$ denote a sampled version of the phase history $E(f,\theta)$ in (8). The damped exponential model is given by

$$E(k,l)=\sum_{m=1}^{M}\tilde{A}_m p_{xm}^k p_{ym}^l, \qquad \begin{matrix} k=-K,\ldots,K-1 \\ l=-L,\ldots,L-1 \end{matrix} \tag{9}$$

where p_{xm} and p_{ym} are the complex modes (poles) describing the exponential behavior of the mth scattering center in the downrange and crossrange dimensions, respectively. Equating (9) to (8) to first order, one arrives at a mapping from parameters in (9) to the physically based parameters in (8). From the signal modes, the estimated slant plane location and α parameter for the scattering center are given by

$$\begin{aligned} \hat{x}_m &= \frac{-\arg\{\hat{p}_{xm}\}c}{4\pi\Delta f}, \qquad \hat{y}_m = \frac{-\arg\{\hat{p}_{ym}\}c}{4\pi f_c\Delta\theta} \\ \hat{\alpha}_m &= \frac{(|\hat{p}_{xm}|-1)f_c}{\Delta f}, \qquad \hat{\beta}_m = \frac{\ln|\hat{p}_{ym}|}{\Delta\theta}. \end{aligned} \tag{10}$$

2) Error in the Reduced Complexity Model: Several authors have suggested that for narrow fractional bandwidths, the power dependence of scattering amplitude as a function of frequency in (8) can be well approximated by a damped complex exponential [2], [34], [16]

$$\left(\frac{jf}{f_c}\right)^{\alpha} \approx j^{\alpha}e^{\gamma f}. \tag{11}$$

For example, the linearly increasing amplitude of flat plate scattering can be approximated by an exponential with $|e^{\gamma}|>1$. We formalize this intuitive approximation in the following theorem. For clarity and simplicity, we state results for the one-dimensional (1-D) range lines, $E(f)$ with θ fixed, and range samples indexed from 0 to $N-1$.

Let $\{D_0,..,D_{N-1}\}$ be samples of superimposed damped exponential signals

$$D_k=\sum_{m=1}^{M}\tilde{A}_m\exp\{(\gamma_m+j\phi_m)k\} \quad k=0,...,N-1 \tag{12}$$

and let H_{de} be the corresponding $P\times Q$ Hankel data matrix

$$H_{de}=\begin{bmatrix} D_0 & D_1 & D_2 & \cdots & D_{Q-1} \\ D_1 & D_2 & D_3 & \cdots & D_Q \\ D_2 & D_3 & D_4 & \cdots & D_{Q+1} \\ \vdots & & & & \vdots \\ D_{P-1} & D_P & D_{P+1} & \cdots & D_{N-1} \end{bmatrix}. \tag{13}$$

The M exponential modes $\exp\{\gamma_m + j\phi_m\}$ can be obtained from the rank M matrix H_{de} by solving a generalized eigenvalue problem using the numerically stable singular value decomposition (SVD) [38]–[40]. For a single θ, let the N frequency samples from the GTD scattering model in (8) be denoted $\{E_0, .., E_{N-1}\}$. Let H denote a $P \times Q$ Hankel data matrix formed from $\{E_0, ..., E_{N-1}\}$, with $\min(P, Q) \geq M$.

Theorem 1: Given a GTD Hankel matrix H, there exist matrices H_{de} and H_{er} such that $H = H_{de} + H_{er}$, and the approximation error H_{er} satisfies the error bound

$$||H_{er}||_2 \leq \sqrt{PQ} \sum_{m=1}^{M} \left| \tilde{A}_m \left[\left(1 + \frac{\text{BW}}{2}\right)^{\alpha_m} - \left(1 - \frac{\text{BW}}{2}\right)^{\alpha_m} \left(1 + \alpha \frac{\Delta f}{f_0}\right)^{(N-1)} \right] \right| \tag{14}$$

where $(f_0, \Delta f)$ are the initial and step frequencies, BW is the sensor fractional bandwidth $\frac{(N-1)\Delta f}{f_0 + N\Delta f/2}$, and $(\tilde{A}_m, \alpha_m)$ are amplitude and geometry of the mth scattering center in (8). Furthermore, H_{de} is a rank M damped exponential signal matrix defined in (12) and (13) whose mode angles ϕ_m are exactly related to range locations via

$$\phi_m = -4\pi \Delta f x_m / c. \tag{15}$$

A proof of the theorem is given in [28]. The theorem generalizes the approximation result in [41] to allow an arbitrary combination of scattering types, rather than only one type of nonpoint scattering. For statistical accuracy of parameter estimates using damped exponential modeling, $Q = N/3$ is often suggested [42], [39], [30].

Theorem 1 shows that the Hankel data matrix formed from GTD scattering model (8) is close to a Hankel data matrix formed from a damped exponential model whose mode angles are exactly specified by the scattering center range parameters. The bound in (14) quantifies closeness. Continuity of eigendecomposition implies that estimated mode angles closely approximate the range parameters, and justifies the use of damped exponential models when the error H_{er} is sufficiently small with respect to noise and clutter. In addition, the result that the range locations found from H_{de} are exactly the range locations from (8), coupled with the error bound (14) computable from radar system properties and scattering constants, motivates the use of the damped exponential model. Consequently, we access a rich literature on damped exponential modeling algorithms for computing parameter estimates.

3) Estimation Algorithms: Adopting the damped exponential model, estimation of attributed scattering centers becomes an exercise in fitting the parametric model to the phase history samples $E(k, l)$. In (9), the curve fit is a nonconvex optimization problem in a high-dimensional space; yet, for damped exponential models there are many available estimation algorithms in the statistical signal processing literature, including 2-D iterative quadratic maximum likelihood (IQML) [43], 2-D method of direction estimation (MODE) [46], 2-D matrix pencil methods [44], and 2-D extensions to total least-squares (TLS)-Prony methods [16], [22]. These algorithms exploit the low-rank property of the (block) Hankel noiseless data matrix, or, equivalently, the property that the M noiseless damped exponentials in (9) are the solutions to an Mth-order, homogeneous, constant coefficient difference equation. A comparison of these methods can be found in [45].

To summarize key results in [45], 2-D IQML gives maximum likelihood parameter estimates, but is computationally and memory intensive; there is no significant computational advantage over estimating parameters using the GTD-based ML method discussed above. The 2-D MODE, 2-D matrix pencil, and 2-D TLS-Prony techniques are 2-D extensions of similar 1-D algorithms, and use subspace-based decomposition of H_{de} or its 2-D extensions. Some of the 2-D extensions are "true 2-D" generalizations; these involve singular value decompositions (SVD's) of very large matrices (e.g. 2000×400 matrices for 64×64 scattering data arrays) and are computationally intensive. However, they have good asymptotic statistical properties because they exploit the 2-D exponential structure in the data. Other 2-D extensions compute separately the downrange modes and crossrange modes using small-dimensional data matrices, and then match the downrange and crossrange modes in some way [22], [46]. These methods are less computationally or memory intensive than the "true 2-D" methods, but they are also less accurate. Moreover, the mode matching step can generate errors, especially for weak modes or low SNR [45].

Statistical analysis of both 1-D [47], [48], [39], [49] and 2-D [22], [43], [50] damped exponential estimators, and corresponding CR bounds [43], [51], are available. The "true 2-D" methods generally outperform the combined 1-D methods because they exploit the damped exponential structure in both dimensions simultaneously. The relative accuracy between these two approaches can be significant—the variance of the location estimates can differ by a factor of 10 or more [52]. We note that these statistical analyses give only a partial guide to estimation performance for radar applications, since the analyses assume the damped exponential model is correct and the noise is additive, white, and Gaussian. The mismatch between the model and noiseless signal affects statistical behavior of parameter estimates. However, from Theorem 1 and the continuity of estimation algorithms, the predictions from statistical analysis are accurate when the radar fractional bandwidth is narrow and scattering centers are separated by two or more Fourier bins [29].

B. Undamped Exponential Model

1) Scattering Model: Similar to the damped exponential model, the undamped exponential model is given by

$$E(k, l) = \sum_{m=1}^{M} \tilde{A}_m e^{j\phi_{xm}k} e^{j\phi_{ym}l} \qquad \begin{matrix} k = 0, \cdots, K-1 \\ l = 0, \cdots, L-1. \end{matrix} \tag{16}$$

From the angles ϕ_{xm} and ϕ_{ym}, the slant plane location of the scattering center is given by

$$x_m = \frac{-\phi_{xm} c}{4\pi \Delta f} \qquad y_m = \frac{-\phi_{ym} c}{4\pi f_c \Delta\theta}. \tag{17}$$

The undamped exponential model is equivalent to the GTD-based model in (8) for the special case of $\alpha_m = \beta_m = 0$. Thus,

the undamped exponential model is obtained by assuming ideal point scattering, i.e., scattering amplitude is independent of both frequency and angle.

2) Approximation Bound: Intuitively, an isotropic, frequency-invariant scattering center model is a good approximation to the GTD model only for small relative bandwidth and very small angular aperture. Such scenarios are encountered with K-band radars and with X-band radars at lower resolution. The following theorem, analogous to Theorem 1, quantifies the approximation error between the GTD model (8) and the undamped exponential model (16). The bound is expressed in terms of system variables, such as bandwidth, target-to-clutter ratio, and frequency sample spacing. We again consider range lines for fixed θ.

Theorem 2: Given a GTD Hankel matrix H, there exist matrices H_{ue} and H_{er} such that $H = H_{ue} + H_{er}$, and the approximation error H_{er} satisfies the error bound

$$||H_{er}||_2 \leq \sqrt{KL}\frac{BW}{2}\sum_{m=1}^{M}\left|\tilde{A}_m\alpha_m\right|\left(\frac{\Delta f}{f_0}\right)^{\alpha_m-1}. \quad (18)$$

Furthermore, H_{ue} is a rank M undamped exponential signal matrix whose mode angles ϕ_m are exactly related to range locations via $\phi_m = -4\pi\Delta f\ x_m/c$.

The proof is given in [28]. We see that the GTD Hankel matrix is close to the undamped exponential Hankel matrix when the undamped exponential model scattering center locations align exactly with the true locations.

3) Estimation Algorithms: There are many estimation algorithms for fitting the model in (16) to the phase history; see, e.g., [53]. The early work of Kennaugh *et al.* [10], [11] used the magnitude of the fast Fourier transform (FFT) followed by a nonlinear peak extraction to identify signal modes; due to its computational simplicity, this approach remains attractive, and variants include order-recursive matched pursuit techniques techniques [54], [55]. These methods were designed for sidelobe suppression for the case of well-separated scattering centers having widely differing amplitudes [56]; consequently, while they locate isolated scattering centers to within less than a Fourier resolution bin at high SNR, these methods are unable to significantly super-resolve closely-spaced scattering centers. More importantly for radar, the methods are biased, and it is often their bias that limits applicability to scattering center extraction [56].

Many signal subspace versions of undamped exponential modeling algorithms are also available [53]. These methods are very similar to corresponding damped exponential subspace methods. Some algorithms exploit the conjugate symmetry property of undamped exponential sequences to slightly improve estimation accuracy for small data sizes or low SNR [53].

C. Model Order Selection

Any estimation procedure for fitting a parametric signal model to measured data must address the critical issue of model order selection; here, choice of M should be motivated by performance of estimated parameters in an ATR system, and not solely by the asymptotic variance of the estimates themselves [57]. For the models in (8), (9), and (16), underestimating M usually results in high bias of the scattering center estimates. For example, an underestimated model order often results in estimating one center in place of two closely located scattering centers on the target. Overestimation of M can result in spurious scattering center estimates and increased variance of the scattering attribute parameters.

Model order estimation techniques for both the damped and undamped exponential models have been developed, primarily for the 1-D modeling case [58]. Additionally, authors of both 1-D and 2-D subspace methods suggest estimating model order by considering the distribution of singular values in the Hankel data matrix. These methods are not well suited to radar scattering center extraction because they are based on either *ad hoc* criteria or information theoretic measures, and are not closely related to probabilities of order misestimation. Moreover, in ATR applications there is a need to associate different costs to model underestimation and overestimation; these costs reflect the need to penalize high parameter bias that results from underestimation (such high bias is undesirable in subsequent feature match processing, for example, [18]). Unfortunately, most existing order selection criteria offer no convenient way to incorporate different costs for undermodeling and overmodeling. The lack of reliable model order estimation techniques and the high bias behavior in parameter estimates have overshadowed parameter variance in the application of parametric feature extraction to radar ATR.

Incorrect model order estimation also adversely affects most ML techniques because initial estimates with high bias (resulting from underestimation of order, for example) are far from the global minimum of the likelihood function; subsequent descent from these initial biased estimates results in convergence to suboptimal local minima [59].

We have developed an order-selecting ML (OSML) algorithm to mitigate these problems [60], [57]. The approach jointly estimates model order and least-squares parameter estimates. The algorithm uses an FFT to initialize a parametric model. Bias resulting from FFT resolution limitation is substantially reduced by splitting FFT peaks into multiple closely located peaks; the number and separation of the split peaks is governed by their associated CR bound resolution limit. Specifically, each FFT peak is split into $n = \frac{2\pi}{\Delta\omega N}$ equal-amplitude peaks (N is the data length), with frequency separations of $\Delta\omega$ chosen as the 95% confidence (based on the CR bound) that two equal-amplitude exponentials can be resolved; see [60] for details. Extraneous modes that may generated by the peak splitting are subsequently eliminated by thresholding amplitudes after the ML descent iteration; this amplitude test can be tied to the probability of false alarm of a scattering center. Thus, the algorithm provides both model order estimation and ML initialization that is within the region of attraction of the global minimum of the likelihood function [60].

Fig. 6 shows the undamped exponential modeling results for both the OSML algorithm and the matrix pencil algorithm [39] applied to scattering center range estimates of X-band radar scattering of an aircraft, simulated using XPatch. The scattering measurements are corrupted by additive white

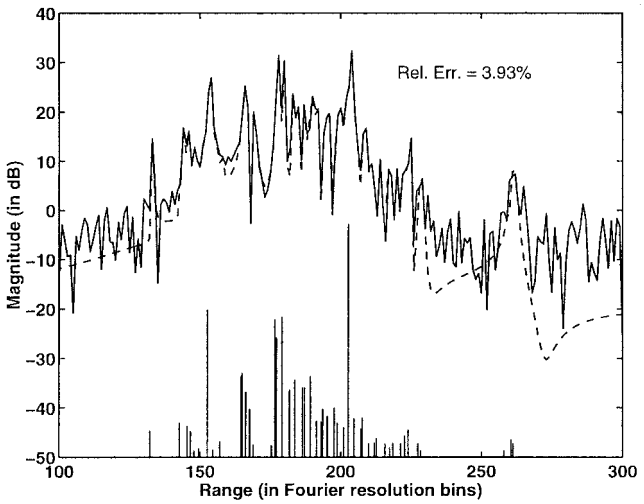

(a)

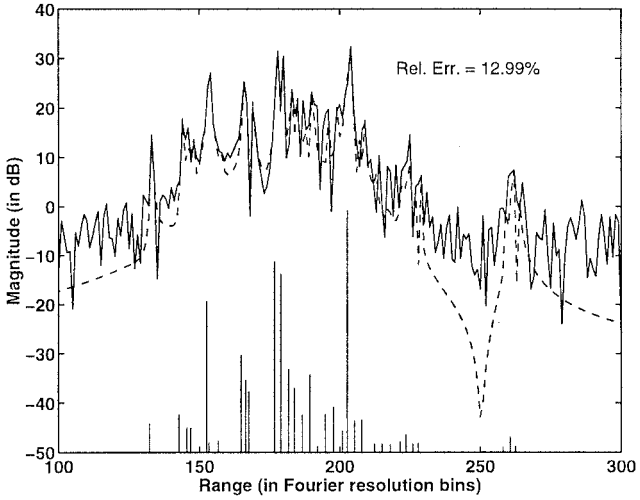

(b)

Fig. 6. Comparison of (a) OSML and (b) matrix pencil methods for range profile modeling. XPatch-generated range profile of an aircraft at X-band, with SNR = 13.89 dB. Solid line: original range profile. Dotted line: range profile reconstructed from scattering center location and amplitude estimates.

Gaussian noise with SNR of 13.89 dB. For illustration, a single aperture angle is considered. For each algorithm we show the original FFT range profile for comparison as a ground truth, and vertical lines to represent the locations and magnitudes of the estimated scattering centers. Also shown is the reconstructed FFT range profile using the estimated scattering parameters (at the FFT resolution). The model order was autoselected as 48 by the OSML method; for matrix pencil both the Akaike information criterion (AIC) and minimum description length (MDL) [61] predicted a model order of thirty-three. (The matrix pencil method with model order 48 also exhibits misestimation of dominant peaks, and a fit error of 8.7%.). We see that the matrix pencil method fails to locate several of the higher energy scattering mechanisms, while the OSML method faithfully estimates all of the scattering centers that are within 26 dB of the peak. In addition, the use the more general damped exponential model in the matrix pencil approach results in almost no difference from Fig. 6(b); this is expected because of the small relative bandwidth of the data—the estimated damping coefficients in the exponential modes are nearly zero. The matrix pencil algorithm, if used as an initial estimate to an ML descent procedure, results in convergence to a suboptimal local minimum because of the high initial bias. Finally, we note that the 3.93% residual error in the OSML estimate agrees very closely with the predicted 3.92% error that would result from perfect modeling of the target in white noise with SNR of 13.89 dB.

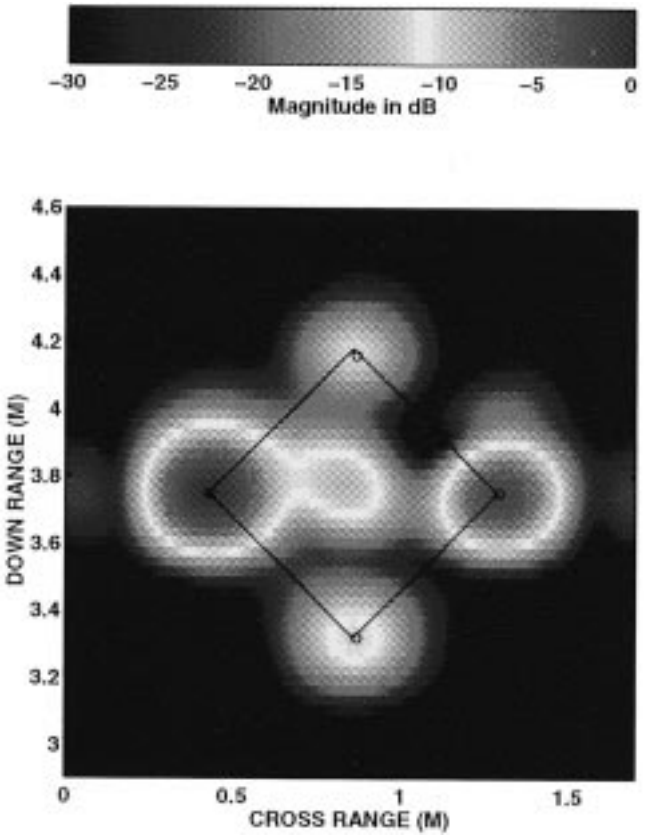

Fig. 7. Inverse SAR image of scattering from 2-ft-square plate. The overlay shows the plate, and circles indicate the estimated scattering center locations.

D. Measured Data

In Fig. 7 we show application of the damped exponential model in (9) and (10) to scattering from a 2-ft-square metal plate measured in The Ohio State University ElectroScience Laboratory anechoic chamber. The data collection parameters are $K = 25$, $L = 5, \Delta\theta = 0.5°$, $\Delta f = 20$ MHz, $f_c = 10$ GHz, and horizontal polarization. The inverse SAR image is formed by the magnitude of the inverse FFT of the Hamming windowed data; the overlay shows the plate, with circles indicating the estimated scattering center locations.

The frequency dispersion parameter, α, is correctly estimated as $\hat{\alpha} = -1$ (corner scattering) for each of the four corners. The six distances between the corners are estimated with an average error of 0.0040 ft, which is $\frac{1}{122}$ the Fourier bin spacing. The maximum error in estimated edge length, as computed from estimated corners, is 0.022 ft (0.045 Fourier bins). The damped exponential model represents the backscattered

energy with 13.0% residual error. We conjecture that most of the error is due to unmodeled spurious scattering from the plate support structure.

IV. Polarimetric Attributes

Polarization diversity in radar measurements allows further description of a scattering center. Fusion of the data from multiple antenna polarizations requires processing of multichannel amplitudes. For a horizontal and vertical polarization basis, and monostatic scattering (i.e., colocated transmit and receive antennas) we form the scattering matrix

$$S(f,\theta)=\begin{bmatrix} S_{hh}(f,\theta) & S_{hv}(f,\theta) \\ S_{vh}(f,\theta) & S_{vv}(f,\theta) \end{bmatrix} \tag{19}$$

where, for example, $S_{vh}(f,\theta)$ gives the amplitude and phase of measured backscatter at frequency f and angle θ for horizontal transmit and vertical receive polarization.

Scattering matrices for many canonical scattering centers are well known [62]. In this section, we use an M-ary generalized likelihood ratio test to classify the measured polarimetric signature of a scattering center. As a byproduct, we obtain the ML estimate of the unknown orientation angle, further describing a scattering center.

A. Physical Model

In general, the scattering matrix S is a function of frequency and angle of incidence. As presented in [5], [3], [22], a scattering model can be used to jointly process multiple polarization channels. A processing gain is realized since measurement of multiple polarizations increases the signal energy. From the scattering models in (8), (9), or (16), we have estimates of the scattering coefficients for a given frequency and angle. For example, from the exponential signal models in (9) and (16) the horizontal transmit and horizontal receive (HH) amplitude coefficient for the mth scattering center is $S_{hh}(f_0,\theta_0)=A_{HH,m}$. Similarly, for the GTD-based model in (8), the mth scattering center has HH amplitude coefficient $S_{hh}(f_c,\theta_0)=A_{HH,m}j^{\alpha_m}$ (cf. (5)).

Alternatively, the scattering may be approximated from complex-valued pixels in pixel registered polarimetric imagery. When using image pixels, each resolution cell is assumed to contain a dominant scattering center whose scattering response is independent of frequency and angle. Further, for time-domain pulse radars, the scattering matrix can be inferred from the complex envelope of the range profiles [63].

The Huynen polarimetric representation [62] expresses a general complex-valued scattering matrix in terms of six parameters physically linked to the geometry of the scatterer

$$S=e^{j\rho}U^{*}(\psi,\tau,\nu)A\begin{bmatrix}1 & 0\\ 0 & \tan^2\gamma\end{bmatrix}U^{H}(\psi,\tau,\nu) \tag{20}$$

where A is the magnitude, ρ is the absolute phase, ψ is the tilt (orientation) angle, τ is the ellipticity angle, ν is the skip angle, and γ is the characteristic angle. The matrix U is unitary. Reviews of polarimetric representations are given in [63] and [64].

We adopt a vector representation of the Huynen model that is more suitable for computation. Assuming monostatic scattering in free space, we invoke reciprocity, $S_{hv}=S_{vh}$, to represent S as the complex-valued triple, $S=[S_{hh}\sqrt{2}S_{hv}S_{vv}]^T$. For each of eight canonical polarimetric signatures, we represent S as

$$S=A_cBb_i(\psi)=A_c\begin{bmatrix}\frac{1}{\sqrt{2}} & \frac{1}{\sqrt{2}} & 0\\ 0 & 0 & 1\\ \frac{1}{\sqrt{2}} & \frac{-1}{\sqrt{2}} & 0\end{bmatrix}b_i(\psi) \tag{21}$$

where $A_c=Ae^{j\rho}$ is a complex amplitude and the 3-by-1 complex vector $b_i(\psi)\in\mathcal{C}^3$ is the ith canonical signature at an orientation angle ψ represented in the basis B for convenience. In Table II we summarize the factorization for eight canonical scattering matrices [65]. The parameters describing absolute phase, amplitude, and orientation angle are modeled as deterministic and unknown. Choice of the remaining Huynen parameters, (τ,ν,γ), defines a canonical form. The parameters are physical descriptors of the target. For example, the skip angle ν is related to the number of bounces of the geometric optics reflected signal; odd bounce mechanisms correspond to $\nu=0°$, whereas even bounce mechanisms correspond to $\nu=\pm 45°$.

TABLE II
Polarimetric Signatures for Canonical Scattering Centers

Scattering Center	$b_i(\psi)$
Trihedral	$\begin{bmatrix}1 & 0 & 0\end{bmatrix}^T$
Dihedral ($a=0$) Narrow Diplane ($a=\frac{1}{3}$) Dipole ($a=1$) Cylinder ($a=3$) Quarter Wave ($a=j$)	$\begin{bmatrix}a & \cos(2\psi) & \sin(2\psi)\end{bmatrix}^T$
Left (Right) Helix	$e^{j2\psi}\begin{bmatrix}0 & 1 & (-)j\end{bmatrix}^T$

B. GLRT Processing

For M canonical target polarization signatures we have M corresponding hypotheses. We have also the null hypothesis, which corresponds to the clutter-only case. By minimizing the Bayes risk, we obtain two Bayes-optimal decision rules: one Neyman–Pearson-type decision rule for detection of canonical targets in clutter and one maximum *a posteriori* (MAP) type rule for classification of detected canonical forms. The $M+1$ hypotheses are

$$H_0: S=n \tag{22}$$

$$H_i: S=A_cBb_i(\psi)+n \qquad \text{i=}1,\cdots,M. \tag{23}$$

For the clutter signal n we adopt an additive, spherically invariant random vector (SIRV) model, which includes Gaussian, K, log-normal and Weibull clutter probability distributions as special cases [66]. The complex clutter random vector is the product of a positive real amplitude a with a complex Gaussian random vector v. Product models have been found to accurately model heavy-tailed forest and terrain clutter [63], [67]–[69]. Let the probability density function for the scalar random variable a be $f(a)$, and let the Gaussian random vector

be zero mean with covariance Σ. Then the probability density function of n can be expressed as

$$f_n(n) = \frac{1}{\pi^3|\Sigma|}\int_0^\infty \frac{f(a)}{a^3}\exp(-n^H\Sigma^{-1}n/a^2)da = F_n(||n||_\Sigma) \tag{24}$$

where $F_n(\cdot)$ is a real-valued, decreasing function of a nonnegative real variable, and $||n||_\Sigma = n^H\Sigma^{-1}n$ is the weighted norm of n.

We assign a Bayes cost to each decision as

$$C_{ij} = \text{Cost}[\text{decide } H_i|H_j] = \begin{cases} 0, & i=j \\ 1, & i\neq j \quad j\neq 0 \\ \eta, & i\neq j \quad j=0. \end{cases} \tag{25}$$

Note that choice of η serves to penalize missed detection differently than misclassifications of the M polarimetric signatures. The Bayes risk is given by

$$\text{Risk} = \sum_{j=0}^{M}\sum_{i=0}^{M} P_j C_{ij} P_{i|j} \tag{26}$$

where P_j is the prior probability of H_j and $P_{i|j}$ is the probability of deciding H_i when H_j is true. The Bayes optimal decision rule partitions the measurement space to minimize the risk and can be expressed as a piecewise linear rule in an M-dimensional space with coordinates [70] given by likelihood ratios

$$\Lambda_k(S) = \frac{P_{S|H_k}(S|H_k)}{P_{S|H_0}(S|H_0)} \qquad k=1,\cdots,M. \tag{27}$$

Two decision rules emerge as a consequence of minimizing the Bayes risk. First, we have the following decision rule for the detection of canonical targets in SIRV clutter:

$$\max_{i=1,\ldots,M}\{P_i\Lambda_i(S)\} \underset{H_0}{\overset{H_1\cup\ldots\cup H_M}{\gtrless}} \eta P_0. \tag{28}$$

Second, we have a decision rule for classifying the scattering center in one of the M classes when H_0 is rejected.

$$\max_{i=1,\cdots,M} P_i\Lambda_i(S) \tag{29}$$

However, the likelihood ratios depend on the unknown target parameters (A,ρ,ψ). A complete Bayes approach would be to integrate $P(S|H_k,(A,\rho,\psi))$ over these parameters using their prior distributions and use this reduced form in the likelihood ratios. In the absence of prior distributions, we adopt a generalized likelihood ratio test (GLRT). That is, we replace the likelihood ratios in (27) with the maximum likelihood ratios, where the unknown (A,ρ,ψ) parameters in (27) are replaced by their maximum likelihood estimates [70].

For equal priors $P_1=\cdots=P_M$, the detection rule in (28) is in the form of a Neyman–Pearson test, as follows:

$$\frac{\max_{i=1,\ldots,M}\left\{F_n(S-\hat{A}_{ci}b_i(\hat{\psi}_i))^H\Sigma^{-1}(S-\hat{A}_{ci}b_i(\hat{\psi}_i))\right\}}{F_n(S^H\Sigma^{-1}S)} \underset{H_0}{\overset{H_1\cup\ldots\cup H_M}{\gtrless}} \eta \tag{30}$$

and the classification rule is in the form of a MAP rule (since F_n is monotone decreasing)

$$i = \arg\min_{i=1,\ldots,M}(S-\hat{A}_{ci}b_i(\hat{\psi}_i))^H\Sigma^{-1}(S-\hat{A}_{ci}b_i(\hat{\psi}_i)) \tag{31}$$

where $\hat{A}_{ci}$ and $\hat{\psi}_i$ are ML estimates for A_{c_i} and ψ_i, respectively. Inserting the ML estimates [65] in (31), the decision rule for classification is

$$i = \arg\max_{i=1,\cdots,M}\left[\sup_{\psi}\frac{|b_i(\psi)^H\Sigma^{-1}S|}{||b_i(\psi)||_\Sigma}\right]. \tag{32}$$

Polarimetric classification of scattering matrices was previously suggested in [71] and [72]; however, (31) and (32) implement the concept in a GLRT by computing ML estimates of amplitude, phase, and orientation angle, and incorporating a SIRV clutter covariance model. The prescreener in (28) is an extension of the binary GLRT in [63] and [73] that classifies each pixel as either dihedral in clutter or as clutter.

The detection rule in (32) admits a simple geometric interpretation and implementation in $\mathcal{C}^3$. Variation of (A_c,ψ) for a canonical polarimetric signature forms the surface of a cone in $\mathcal{C}^3$. The MAP polarimetric classification rule in (32) selects the target cone closest to the measured scattering matrix S using a distance weighted by the inverse of the clutter covariance, Σ^{-1}. The weighted projection onto the cone also yields ML estimates of orientation, amplitude and phase, $(\hat{\psi},\hat{A},\hat{\rho})$ [65]. For computation, the 1-by-3 complex vectors $\frac{b_i(\psi)^H\Sigma^{-1}}{||b_i(\psi)||_\Sigma}$ in (32) can be precomputed for sampled values of ψ, leaving only inner products to be computed for classification of a measured signature, S. A sampling increment of 5°, together with target symmetries, requires evaluation of only 165 inner products in $\mathcal{C}^3$ to implement (32).

As with other scattering center attributes, an associated uncertainty can be computed for each polarimetric signature. For each scattering center hypothesis, the relative certainties in classification are given by the posterior probabilities $P(H_i|S), i=1,\cdots,M$. Computation of $P(H_i|S)$ requires integration over all values of the unknown parameters (A,ρ,ψ) and is therefore computationally burdensome. Hence, we replace the distributions with a point mass assumption at their maximum likelihood values

$$P(S|H_i) = F_n((S-\hat{A}_c b_i(\hat{\psi}))^H\Sigma^{-1}(S-\hat{A}_c b_i(\hat{\psi})) = F_n(d_k^{min}) \tag{33}$$

where d_k^{min} is the minimum weighted distance of scattering center S to kth canonical target cone. Then, using Bayes Rule, we compute the *a posteriori* probabilities as

$$P(H_k|S) = \frac{P_k F_n(d_k^{min})}{\sum_{i=1}^{M} P_i F_n(d_i^{min})}. \tag{34}$$

C. Polarimetric GLRT Example

Fig. 8 illustrates application of the polarimetric GLRT to ultrawide bandwidth rail SAR data collected at Ohio State University Big Ear Radio Observatory (237–1558 MHz, 120-ft linear aperture). Fig. 8(a) shows the PWF image of a 240-ft-by-120-ft forested scene (0.75-ft pixel spacing in range and crossrange). Illumination is from the left. The subimages in Fig. 8(b)–(d) show classification of the three dominant

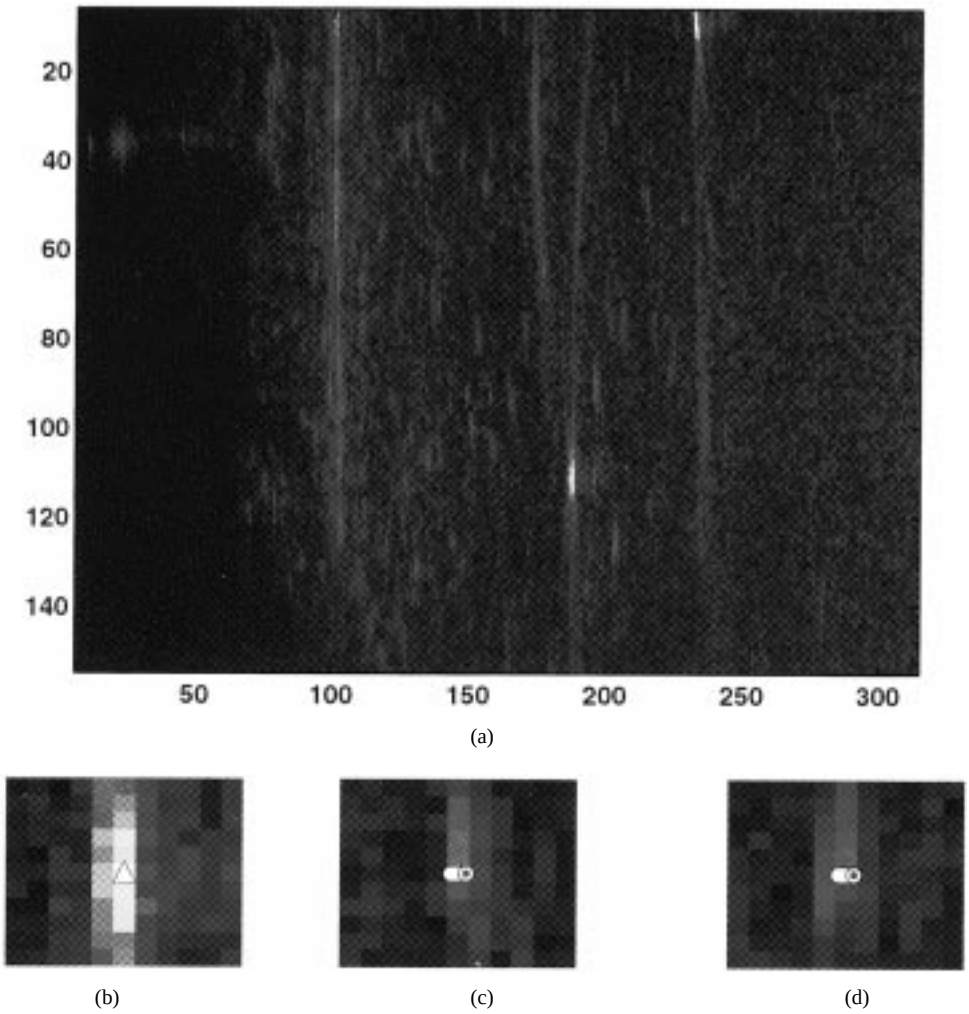

Fig. 8. Polarimetric detection results for three subregions; superimposed icons denote detected signatures.

scattering centers in the 30-by-50 pixel region centered on pixel [195 110]; the superimposed icons depict one trihedral and two cylinders. Survey data indicates one 4-ft trihedral and two trees exceeding 14 in diameter at breast height, respectively, at the corresponding locations in the scene.

V. Conclusions

A high-frequency approximation of electromagnetic scattering as provided by the GTD shows that the scattering response of an object is well approximated as a sum of scattering centers. The GTD model remains accurate for targets that are larger than a few wavelengths in extent. For such targets, an attributed scattering center model provides a parsimonious, physically relevant description of the backscattered signal.

In this paper, we presented a feature extraction approach in which physically based scattering models are used to analyze SAR data. Model parameters are estimated from the measurements, and the estimated values describe attributes of each scattering center. We proposed a scattering model derived from the GTD and described a nonlinear least-squares estimator for the model parameters. The estimated scattering center attributes include location, fully polarimetric amplitudes, aspect-dependent amplitude taper, and geometric type. Additionally, we discussed two reduced complexity scattering models, the damped exponential and undamped exponential models. Parameters in the reduced complexity models were related to the physically based GTD model parameters, and we surveyed relevant results from the statistical signal processing literature. Further, we quantified the modeling error incurred in adopting the reduced complexity models. An order-selecting ML algorithm for scattering center estimation was proposed for addressing the important issue of model order estimation. Finally, we presented an M-ary GLRT detector for fusion of multiple polarization scattering data in non-Gaussian, spherically invariant random clutter; the detector classifies the polarimetric signature of each scattering center.

Scattering centers, as described by estimated attributes, offer a rich set of discriminating features for SAR ATR. However, such features have limitations and cannot serve as the only vocabulary for ATR. Scattering centers should be augmented by additional features describing, for example, shadow, context, and image texture—behavior not incorporated in a scattering center model. In addition, parametric scattering center extraction is computationally more demanding than traditional image formation and is therefore inappropriate for a prescreening detection function. Related to computational cost

are the numerical challenges of model order selection, nonconvex optimization, and complexity in modeling the angular dependence of scattering behavior. Finally, some scattering attributes are not universally applicable. For example, the α descriptor of geometry requires large relative bandwidth (or very high SNR) for reliable estimation, as depicted in Fig. 5. Likewise, the polarimetric classification of scattering centers requires multipolarization measurements with proper calibration and registration.

Attributed scattering center models exploit scattering phenomenology that is not accessed through SAR imaging formation. Frequency, aspect and polarization dependent scattering behavior can be jointly processed to provide descriptive, high-resolution analysis of regions of interest. The extracted attributes and associated statistical uncertainty offer a predictable, compact characterization of single and multiple polarization SAR data. Research in attributed parametric modeling of scattering continues, and several generic parametric modeling issues remain. First, the unified theory of diffraction offers improved modeling of the aspect dependence of scattering centers. Second, time-domain modeling is of interest for ultrawideband pulse radar systems. Third, development continues toward computationally efficient parameter estimation methods that appropriately select model order and avoid high parameter bias caused by inaccurate initialization. Modeling of the complex image potentially offers clutter suppression and approximate partitioning of scatterers and, hence, reduced computational complexity.

ACKNOWLEDGMENT

The authors gratefully acknowledge many fruitful discussions with D.-M. Chiang, R. Dilsavor, E. Ertin, M. Gerry, and J. Ying.

REFERENCES

[1] J. B. Keller, "Geometrical theory of diffraction," *J. Opt. Soc. Amer.*, pp. 116–130, Jan. 1962.
[2] M. P. Hurst and R. Mittra, "Scattering center analysis via Prony's method," *IEEE Trans. Antennas Propagat.*, vol. AP-35, pp. 986–988, Aug. 1987.
[3] W. M. Steedly and R. L. Moses, "High resolution exponential modeling of fully polarized radar returns," *IEEE Trans. Aerosp. Electron. Syst.*, vol. 27, pp. 459–469, May 1991.
[4] S. Scarborough, "Ultrawideband radar imaging and the diagnosis of scattering centers," Master's thesis, The Ohio State Univ., Columbus, 1990.
[5] N. F. Chamberlain, E. K. Walton, and F. D. Garber, "Radar target identification of aircraft using polarization-diverse features," *IEEE Trans. Aerosp. Electron. Syst.*, vol. 27, pp. 58–67, Jan. 1991.
[6] D. E. Dudgeon and R. T. Lacoss, "An overview of automatic target recognition," *Lincoln Lab. J.*, vol. 6, no. 1, pp. 3–10, 1993.
[7] F. D. Garber, N. F. Chamberlain, and Ö. Snorrason, "Time-domain and frequency-domain feature selection for reliable radar target identification," in *Proc. IEEE 1988 Nat. Radar Conf.*, Ann Arbor, MI, Apr. 1988, pp. 79–84.
[8] N. Tseng, "A very efficient RCS data compression and reconstruction technique," Master's thesis, The Ohio State Univ., Columbus, 1992.
[9] L.-C. Chang, "Removal of undesired scattering centers using a radar image technique," Master's thesis, The Ohio State Univ., Columbus, 1993.
[10] E. M. Kennaugh and R. L. Cosgriff, "The use of impulse response in electromagnetic scattering problems," in *Proc. 1958 IRE Nat. Convention Rec.*, pp. 72–77.
[11] E. M. Kennaugh and D. L. Moffatt, "Transient and impulse response approximation," *Proc. IEEE*, vol. 53, pp. 893–901, Aug. 1965.
[12] R. T. Compton, Jr., "Two-dimensional imaging of radar targets with the MUSIC algorithm," Tech. Rep.719267-14, The Ohio State Univ., Dept. Electr. Eng., ElectroSci. Lab., Columbus, Dec. 1987.
[13] D. F. DeLong and G. R. Benitz, "Extensions of high definition imaging," in *Proc. SPIE Int. Symp. Algorithms Synth. Aperture Radar Imagery II*, vol. 2487, D. A. Giglio, Ed., Orlando, FL, Apr. 1995, pp. 165–180.
[14] I. J. Gupta, "High-resolution radar imaging using 2-D linear prediction," *IEEE Trans. Antennas Propagat.*, vol. 42, pp. 31–37, Jan. 1994.
[15] R. Carrière and R. L. Moses, "High resolution radar target modeling using a modified Prony estimator," *IEEE Trans. Antennas Propagat.*, vol. 40, pp. 13–18, Jan. 1992.
[16] J. J. Sacchini, "Development of two-dimensional parametric radar signal modeling and estimation techniques with application to target identification," Ph.D. dissertation, The Ohio State Univ., Columbus, Mar. 1992.
[17] Y. Hua, F. Baqai, Y. Zhu, and D. Heilbronn, "Imaging of point scatterers from step frequency ISAR data," *IEEE Trans. Aerosp. Electron. Syst.*, vol. 29, pp. 195–205, Jan. 1993.
[18] P. B. Silverstein, O. S. Sands, and F. D. Garber, "Radar target classification and interpretation by means of structural descriptions of backscatter signals," *IEEE AES Syst. Mag.*, vol. 6, pp. 3–7, May 1991.
[19] ARPA/SAIC Syst. Architect. Study Grp., "Model-driven automatic target recognition," Oct. 1994.
[20] R. G. Kouyoumjian and P. H. Pathak, "A uniform geometrical theory of diffraction for an edge in a perfectly conducting surface," *Proc. IEEE*, vol. 62, pp. 1448–1461, Nov. 1974.
[21] C. A. Balanis, *Advanced Engineering Electromagnetics*. New York: Wiley, 1989.
[22] J. J. Sacchini, W. M. Steedly, and R. L. Moses, "Two-dimensional Prony modeling and parameter estimation," *IEEE Trans. Signal Processing*, vol. 41, pp. 3127–3137, Nov. 1993.
[23] D. C. Munson and R. L. Visentin, "A signal processing view of strip-mapping synthetic aperture radar," *IEEE Trans. Acoust., Speech, Signal Processing*, vol. 37, pp. 2131–2147, 1989.
[24] D. A. Ausherman *et al.*,"Developments in radar imaging," *IEEE Trans. Aerosp. Electron. Syst.*, vol. 20, pp. 363–398, July 1984.
[25] R. M. Lewitt, "Reconstruction algorithms: Transform methods," *Proc. IEEE*, vol. 71, pp. 390–408, Mar. 1983.
[26] D.-M. Chiang and L. C. Potter, "GTD scattering: Least-squares estimators, approximate models and statistical analysis," SPANN Lab. Tech. Rep. TR-95-07, The Ohio State Univ., Columbus, Oct. 1995.
[27] P. Stoica and T. Söderström, "On reparametrization of loss functions used in estimation and the invariance principle," *Signal Process.*, vol. 17, pp. 383–387, 1989.
[28] D.-M. Chiang, "Parametric signal processing techniques for model mismatch and mixed parameter estimation," Ph.D. dissertation, The Ohio State Univ., Columbus, 1996.
[29] L. C. Potter, D.-M. Chiang, R. Carrière, and M. J. Gerry, "A GTD-based parametric model for radar scattering," *IEEE Trans. Antennas Propagat.*, vol. 43, pp. 1058–1067, Oct. 1995.
[30] W. M. Steedly, C. J. Ying, and R. L. Moses, "Statistical analysis of TLS-based Prony techniques," *Automatica*, vol. 30, pp. 115–129, Jan. 1994.
[31] ———, "Resolution bound and detection results for scattering centers," in *Proc. 1992 Int. Radar Conf.*, Brighton, UK, Oct. 1992, pp. 518–521.
[32] W. Leeper, "Identification of scattering mechanisms from measured impulse response signatures of several conducting objects," Master's thesis, The Ohio State Univ., Columbus, 1984.
[33] R. L. Moses and R. Carrière, "Parametric modeling of radar targets using canonical scattering centers," Tech. Rep. 719267-13, The Ohio State Univ., Dept. Elect. Eng., ElectroSci. Lab., Columbus, Dec. 1987.
[34] R. Carrière and R. Moses, "Canonical scattering analysis of radar targets," in *Proc. 1991 IEEE Int. Conf. Syst. Eng.*, Dayton, OH, Aug., 1991, pp. 13–16.
[35] M. J. Gerry and E. K. Walton, "Analysis of amplitude dispersion in radar scattering using preconditioned linear prediction," in *Proc. 1994 AMTA Symp.*, Oct. 1994.
[36] A. Moghaddar, Y. Ogawa, and E. K. Walton, "Estimating the time-delay and frequency decay parameter of scattering components using a modified MUSIC algorithm," *IEEE Trans. Antennas Propagat.*, vol. 42, pp. 1412–1418, Oct. 1994.
[37] W. M. Steedly, C. J. Ying, and R. L. Moses, "A modified TLS-Prony method using data decimation," in *Proc. SPIE OE/AEROSPACE Sci. Sensing Conf.*, Orlando, FL, Apr. 1992.
[38] S. Y. Kung, K. S. Arun, and D. V. B. Rao, "State-space and singular-value decomposition-based approximation methods for the harmonic retrieval problem," *J. Opt. Soc. Amer.*, vol. 73, pp. 1799–1811, Dec. 1983.
[39] Y. Hua and T. K. Sarkar, "Matrix pencil method for estimating parameters of exponentially damped/undamped sinusoids in noise," *IEEE*

Trans. Acoust., Speech, Signal Processing, vol. 38, pp. 814–824, May 1990.
[40] B. D. Rao and K. S. Arun, "Model based processing of signals: A state space approach," *Proc. IEEE*, vol. 80, pp. 283–309, Feb. 1992.
[41] M. L. Walker and J. W. Helton, "Application of signal subspace algorithms to scattered geometric optics and edge-diffracted signals," *IEEE Trans. Signal Processing*, vol. 42, pp. 2217–2226, Sept. 1994.
[42] H. Clergeot, S. Tressens, and A. Ouamri, "Performance of high resolution frequencies estimation methods compared to the Cramér–Rao bound," *IEEE Trans. Acoust., Speech, Signal Processing*, vol. 37, pp. 1703–1720, Nov. 1989.
[43] M. P. Clark and L. L. Scharf, "Two-dimensional modal analysis based on maximum likelihood," *IEEE Trans. Signal Processing*, vol. 42, pp. 1443–1451, June 1994.
[44] Y. Hua, "Estimating two-dimensional frequencies by matrix enhancement and matrix pencil," *IEEE Trans. Signal Processing*, vol. 40, pp. 2267–2280, Sept. 1992.
[45] C. J. Ying, L. Potter, and R. Moses, "Complex SAR phase history modeling using two dimensional parametric estimation techniques," in *Proc. Algorithms Synthet. Aperture Radar Imagery III, 1996 SPIE Aerosp./Defense Sensing Dual-Use Photonics Symp.*, Apr. 1996.
[46] J. Li, P. Stoica, and D. Zheng, "An efficient algorithm for two-dimensional frequency estimation," Tech. Rep. CTH-TE-24, Chalmers Univ. Technol., Sweden, Sept. 1994.
[47] Y. Bresler and A. MacKovski, "Exact maximum likelihood parameter estimation of superimposed exponential signals in noise," *IEEE Trans. Acoust., Speech, Signal Processing*, vol. ASSP-34, pp. 1081–1089, Oct. 1986.
[48] B. D. Rao, "Perturbation analysis of an SVD-based linear prediction method for estimating the frequencies of multiple sinusoids," *IEEE Trans. Acoust., Speech, Signal Processing*, vol. 36, pp. 1026–1035, July 1988.
[49] W. M. Steedly, C. J. Ying, and R. L. Moses, "A modified TLS-Prony method using data decimation," *IEEE Trans. Signal Processing*, vol. 42, pp. 2292–2303, Sept. 1994.
[50] H. Yang and Y. Hua, "Statistical analysis of an eigendecomposition based method for 2-D frequency estimation," *Automatica*, vol. 30, pp. 157–168, Jan. 1994.
[51] W. M. Steedly and R. L. Moses, "The Cramér–Rao bound for pole and amplitude estimates of damped exponential signals in noise," *IEEE Trans. Signal Processing*, vol. 41, pp. 1305–1318, Mar. 1993.
[52] M. P. Clark, "Cramèr–Rao bounds for 2-D deterministic modal analysis," in *Proc. 27th Asilomar Conf. Signals Syst. Comput.*, Pacific Grove, CA, Nov. 1993, pp. 1151–1156.
[53] P. Stoica, "List of references on spectral line analysis," *Signal Process.*, vol. 31, no. 3, pp. 329–340, Apr. 1993.
[54] S. R. DeGraaf, "SAR image enhancement via adaptive polarization synthesis and polarimetric detection performance," in *Proc. Polarimetric Technol. Workshop*, vol. I.1, Redstone Arsenal, AL, Aug. 1988, pp. 615–631.
[55] J. Tsao and B. D. Steinberg, "Reduction of sidelobe and speckle artifacts in microwave imaging: The CLEAN technique," *IEEE Trans. Antennas Propagat.*, vol. 36, pp. 543–556, Apr. 1988.
[56] S. R. DeGraaf, "Parametric estimation of complex 2-D sinusoids," Tech. Rep. OSL-90-6383, ERIM, Ann Arbor, MI, 1990.
[57] C. J. Ying, L. C. Potter, and R. L. Moses, "On model order determination for complex exponential signals: Performance of an FFT-initialized ML algorithm," in *Proc. 7th Signal Processing Workshop Stat. Signal and Array Processing*, Quebec, Canada, June 1994.
[58] F. Gustafsson and H. Hjalmarsson, "21 ML estimators for model selection," *Automatica*, submitted for publication.
[59] M. P. Pepin, M. P. Clark, and J. Li, "On the applicability of 2-D damped exponential models to synthetic aperture radar," in *Proc. Int. Conf. Acoust., Speech, Signal Processing*, Detroit, MI, May, 1995, pp. 2149–2152.
[60] C. J. Ying and R. L. Moses, "On model order determination of complex exponential signals," in *Proc. 10th IFAC Symp. Syst. Identif.*, Copenhagen, Denmark, July, 1994.
[61] V. U. Reddy and L. S. Biradar, "SVD-based information theoretic criteria for detection of the number of damped/undamped sinusoids and their performance analysis," *IEEE Trans. Signal Processing*, vol. 41, pp. 2872–2881, Sept. 1993.
[62] J. R. Huynen, "Phenomenological theory of radar targets," Ph.D. dissertation, Tech. Univ., Delft, The Netherlands, 1970.
[63] R. L. Dilsavor, "Detection of target scattering centers in terrain clutter using an ultra-wideband, fully-polarimetric synthetic aperture radar," Ph.D. dissertation, The Ohio State Univ., Columbus, Sept. 1993.
[64] D. Giuli, "Polarization diversity in radars," *Proc. IEEE*, vol. 74, pp. 245–269, Feb. 1986.
[65] E. Ertin and L. C. Potter, "Polarimetric classification of scattering centers," in *Proc. Algorithms Synthet. Aperture Radar Imagery III, 1996 SPIE Aerosp./Defense Sensing Dual-Use Photonics Symp.*, Apr. 1996.
[66] M. Rangaswamy, D. Weiner, and A.Öztürk, "Non-Gaussian random vector identification using spherically invariant random processes," *IEEE Trans. Aerosp. Electron. Syst.*, vol. 29, pp. 111–124, Jan. 1993.
[67] H. Zien, "Clutter statistics and detection of targets in ultra-wideband synthetic aperture radar imagery," Master's thesis, Ohio State Univ., Mar. 1995.
[68] L. M. Novak, M. C. Burl, R. D. Chaney, and G. J. Owirka, "Optimal processing of polarimetric synthetic-aperture radar imagery," *Lincoln Lab. J.*, vol. 3, pp. 273–290, 1990.
[69] S. H. Yueh *et al.*,"K-distribution and polarimetric terrain radar clutter," *J. Electromag. Waves Applic.*, vol. 3, no. 8, pp. 747–768, 1989.
[70] H. L. V. Trees, *Detection, Estimation, and Modulation Theory: Part I*. New York: Wiley, 1968.
[71] N. F. Chamberlain, "Recognition and analysis of aircraft targets by radar, using structural pattern representations derived from polarimetric signatures," Ph.D. dissertation, The Ohio State Univ., Columbus, June 1989.
[72] W. L. Cameron and L. K. Leung, "Feature motivated polarization scattering matrix decompositions," in *Proc. IEEE Int. Radar Conf.*, 1990, pp. 549–557.
[73] V. Larson and L. Novak, "Polarimetric subspace target detector for SAR data based on the huynen dihedral model," in *Proc. SPIE Int. Symp. Algorithms Synthet. Aperture Radar Imagery II*, vol. 2487, D. A. Giglio, Ed., Orlando, FL, Apr. 1995, pp. 235–250.

Lee C. Potter (S'89–M'90) received the B.E. degree from Vanderbilt University, Nashville, TN, and the M.S. and Ph.D. degrees from the University of Illinois, Urbana, all in electrical engineering.

Since 1991, he has been with the Department of Electrical Engineering, The Ohio State University, Columbus, where he is Associate Professor. His research interests include signal processing and constrained inverse problems with application to radar target recognition, image coding, and electrocardiography.

Dr. Potter is a 1993 recipient of the College of Engineering MacQuigg Award for Outstanding Teaching.

Randolph L. Moses (S'78–M'85–SM'90) received the B.S., M.S., and Ph.D. degrees in electrical engineering from Virginia Polytechnic Institute and State University, Blacksburg, in 1979, 1980, and 1984, respectively.

During the summer of 1983 he was a SCEEE Summer Faculty Research Fellow at Rome Air Development Center, Rome, NY. From 1984 to 1985 he was with Eindhoven University of Technology, The Netherlands, as a NATO Post-doctoral Fellow. Since 1985 he has been with the Department of Electrical Engineering, The Ohio State University, Columbus, and is currently a Professor there. During 1994–1995, he was on sabbatical leave as a visiting researcher at the System and Control Group, Uppsala University, Sweden. His research interests are in digital signal processing, and include parametric time series analysis, radar signal processing, sensor array processing, and system identification.

Dr. Moses served on the Technical Committee on Statistical Signal and Array Processing of the IEEE Signal Processing Society from 1991–1994. He is a member of Eta Kappa Nu, Tau Beta Pi, Phi Kappa Phi, and Sigma Xi.